Advanced Course and Workshop on Blood Flow
BF 2005 – (pp.361–402) – Warsaw, 2005.

Mathematical and Numerical Modelling of Cardiovascular Flows

Jacek Szumbarski[1)] and Jeremi K. Mizerski[2)]

[1)] *Department of Aerodynamics, Warsaw University of Technology*
jasz@meil.pw.edu.pl

[2)] *2nd Department of Cardiosurgery, Institute of Cardiology*
ul. Alpejska 42, 04-628 Warsaw, Poland
jeremi@data.pl

The rudiments of the numerical simulations of flows in domains relevant to haemodynamic applications are provided. In the first part of these notes, the problem of adequate modeling of the boundary conditions is addressed. In is argued that "classical" repertoire of such conditions is not sufficient and more general approach of the "deficient" formulations of the inlet/outlet conditions should be resorted. In the second part of the notes, a detailed description of the spectral element implementation of the Navier-Stokes solver using the formulation with "deficient" inlet/outlet conditions is given. Results of the computations presented in the notes include some test cases as well as the pulsatile flows in the model of the Blalock-Taussig shunt. The latter case is also considered in the third part of the notes, where the results of the numerical simulations obtained with the commercial package Fluent 6.2 are presented.

Key words: *Navier-Stokes equation, spectral elements, deficient inlet/outlet conditions, Blalock-Taussig shunt, cardiovascular flows*

Introduction

These notes have been written on the basis of the authors' lecture during BF2005 meeting and they consist of three parts. In the first part, we summarize the basic governing equations and discuss the problem of the boundary conditions, which can be consistently set for a flow problem, when different forms of the weak velocity/pressure formulation are used. The problem of adequate modeling of the inlet and outlet conditions is discussed in this framework. We provide arguments that standard repertoire of the boundary conditions is not sufficient to perform realistic simulations of pulsatile flows

in cardiovascular systems. Next, an alternative approach to inlet/outlet conditions, introduced by Heywood et al. [12] and improved by Formaggia et al. [24], is explained in some details. The advantages of this new method in the contexts of haemodynamic simulations are shortly discussed.

The second part of the lecture is devoted to a detailed presentation of the numerical method design and implemented by the authors. The solution method is based on the weak formulation of the initial-boundary problem for the governing equation, where new generalized approach to inlet/outlet conditions is incorporated. The problem of discretization in time and space (using spectral elements) is discussed in some details. Some particular efficiency-improving algorithms are described. Finally, the results of numerical tests are presented and encountered difficulties are demonstrated.

In the third part, we present results of numerical simulations of the Blalock-Taussig shunt obtained by Jeremi Mizerski in his doctoral thesis with the commercial CFD package Fluent 6.2, [25]. It has been found rather difficult to find program and parameter setting, which ensure efficient and accurate results. We show Fluent screenshots demonstrating the applied settings, which resulted in successful calculations. The quasi-compressibility effect of the used solver is demonstrated by evaluation of the balance of volumetric flow rates at all inlets and outlets to the computational domain. Nevertheless, it is argued that obtained results, especially flow patterns, are medically relevant and useful.

1. General Mathematical Issues

1.1. Mathematical Model of a Viscous Incompressible Flow

The governing equations for an incompressible fluid flow stem from two basic principles of classical mechanics of continuum: the mass conservation and the second Newton's law. They are formulated for a fluid region, i.e. for the moving fluid portion consisting of the fixed set of fluid elements (or particles). Originally, the governing equations have the form of integral balances. For sufficiently regular fields we can apply the Reynolds transport theorem and obtain the flow description in terms of partial differential equations. This standard procedure can be found in any handbook on the fluid mechanics. In particular, we recommend excellent handbooks [1,2], also the report [21].

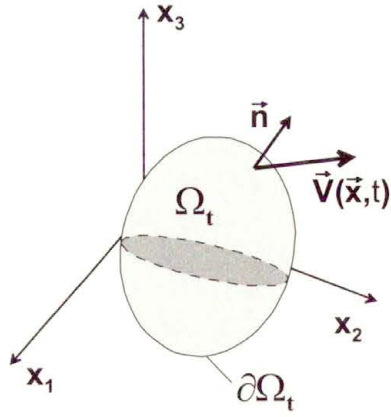

FIGURE 1. The volume of fluid and notation used in text

- Mass conservation $\Rightarrow$ the continuity equation:

$$\frac{d}{dt}\int\limits_{\Omega_t} \rho d\mathbf{x} = 0 \quad \Rightarrow \quad \partial_t \rho + \nabla \cdot (\rho \mathbf{u}) = 0 \quad \Rightarrow \quad \nabla \cdot \mathbf{u} = 0. \tag{1.1}$$

- 2^{nd} Newton's law $\Rightarrow$ the momentum equation (the equation of motion):

$$\frac{d}{dt}\int\limits_{\Omega_t} \rho \mathbf{u} d\mathbf{x} = \int\limits_{\Omega_t} \rho \mathbf{g} d\mathbf{x} + \int\limits_{\partial\Omega_t} \mathbf{T}\mathbf{n} ds$$

$$\Downarrow$$

$$\rho \left[\partial_t \mathbf{u} + (\mathbf{u} \cdot \nabla)\, \mathbf{u}\right] = \mathrm{Div}\, \mathbf{T} + \rho \mathbf{g}. \tag{1.2}$$

Here $\mathbf{u}$ is the velocity field, p is the static pressure field and ρ denotes the (fixed) fluid density. The symbol $\mathbf{T}$ denotes the stress tensor, while $\mathbf{g}$ is the external field of the body force. If the $\mathbf{g}$ field is potential (like a gravitational field, for instance) then the body force term can be included into the pressure term.

An equivalent form of the momentum equation for an incompressible fluid can be written as

$$\rho \partial_t \mathbf{u} + \mathrm{Div}\, (\rho \mathbf{u} \otimes \mathbf{u} - \mathbf{T}) = \rho \mathbf{g}. \tag{1.3}$$

The component wise form of the momentum equation in the Cartesian coordinate system is

$$\rho \partial_t u_j + \rho \sum_{k=1}^{3} u_k \partial_{x_k} u_j - \sum_{k=1}^{3} \partial_{x_k} T_{jk} = \rho g_j. \tag{1.4}$$

In order to obtain a mathematically complete description of the fluid motion, a constitutive relation has to be defined. This is a relation between stresses and kinematics. In is generally accepted that cardiovascular flows in large and medium-sized arteries can be adequately simulated using basic Newtonian or generalized Newtonian models of fluid rheology. The basic ingredient in these models is the deformation rate tensor

$$D = \frac{1}{2}\left(\nabla \mathbf{u} + \nabla \mathbf{u}^T\right), \quad D_{jk} = \frac{1}{2}(\partial_{x_k} u_j + \partial_{x_j} u_k). \tag{1.5}$$

The stress tensor is now defined as follows

$$\mathbf{T} = -p\mathbf{I} + 2\mu\mathbf{D}, \quad T_{jk} = -p\delta_{jk} + \mu(\partial_{x_k} u_j + \partial_{x_j} u_k) \tag{1.6}$$

where μ [kg/(m s)] is the dynamic viscosity of the fluid. In the basic Newtonian model, the viscosity is assumed constant, meaning it does not depend on the flow kinematics. In such case, the momentum equation can be written in several equivalent forms, namely

$$\begin{aligned} \rho\left[\partial_t \mathbf{u} + (\mathbf{u}\cdot\nabla)\,\mathbf{u}\right] &= -\nabla p + 2\mu\nabla\cdot\mathbf{D} + \rho\mathbf{g}, \\ \rho\left[\partial_t \mathbf{u} + (\mathbf{u}\cdot\nabla)\,\mathbf{u}\right] &= -\nabla p + \mu\Delta\mathbf{u} + \rho\mathbf{g}, \\ \rho\left[\partial_t \mathbf{u} + (\mathbf{u}\cdot\nabla)\,\mathbf{u}\right] &= -\nabla p - \mu\nabla\times(\nabla\times\mathbf{u}) + \rho\mathbf{g}. \end{aligned} \tag{1.7}$$

Assuming a fixed viscosity of blood is not feasible if excessive areas of very law shear rate appear persistently within the flow domain. In such case, one can switch to one of the generalized Newtonian models, which accounts for a shear-thinning property of blood. In more complicated situations, the application of even more sophisticated viscoelastic models may occur necessary. Detailed exposition of these topics can be found in the lecture notes [20] (the lectures by Adelia Sequeira and Robert Owens) and references cited therein.

The generalized Newtonian models are based on the relation (1.6) between stress and deformation, but the viscosity in now considered to be shear-dependent. Thus, the constitutive relation can be expressed in the form of

$$\mathbf{T} = -p\mathbf{I} + 2\mu\left(\dot{\gamma}\right)\mathbf{D} \tag{1.8}$$

where the strain rate $\dot{\gamma}$ is the frame-invariant quantity defined as follows

$$\dot{\gamma} = \sqrt{2\mathrm{tr}(\mathbf{D}^2)} = \sqrt{2\mathbf{D}:\mathbf{D}} = \sqrt{2\sum_{i,j=1}^{3} D_{ij}^2} = \sqrt{2}\,\|D\|_F \tag{1.9}$$

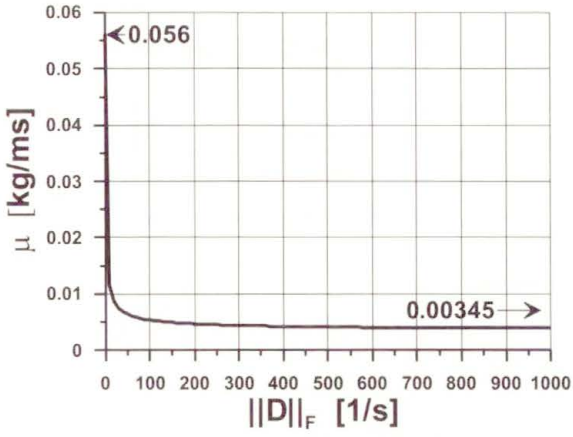

FIGURE 2. Carreau-Yasuda model as used by A. Sequeira and S. Deparis, [20]

In the above, the symbol $\|\mathbf{D}\|_F$ denotes the Frobenius norm of the deformation rate tensor.

As an example consider the Carreau-Yasuda model of a shear-thinning fluid. The formula for the viscosity is given as

$$\mu(\dot{\gamma}) = \mu_\infty + (\mu_0 - \mu_\infty)\left(1 + \lambda\dot{\gamma}^2\right)^\alpha \tag{1.10}$$

where μ_0 and μ_∞ denote the values of the dynamic viscosity in the limit of vanishing and infinite shear rate, respectively. In Fig. 2, the variation of the viscosity for the parameter values ($\mu_0 = 0.056\,\mathrm{kg\,m^{-1}s^{-1}}$), $\mu_\infty = 0.00345\,\mathrm{kg\,m^{-1}s^{-1}}$, $\alpha = -0.3216$, $\lambda = 3.313\,\mathrm{s}$) chosen by Sequeira and Deparis [20] is shown.

1.2. Boundary Conditions for Incompressible Viscous Fluid Flows

In this paragraph we will discuss the problem of the boundary condition, which can be consistently enforced in the incompressible flow of a viscous fluid. Our exposition closely follows the problem description provided by Max Gunzburger in his excellent book [5] on finite element methods. The general idea is to consider various possible forms of the weak (variational) formulations of the governing equations and see what sort of the boundary information can be a priori assumed.

Consider an abstract computational domain Ω. Let the boundary $\partial\Omega$ be divided into parts as shown in the Fig. 3.

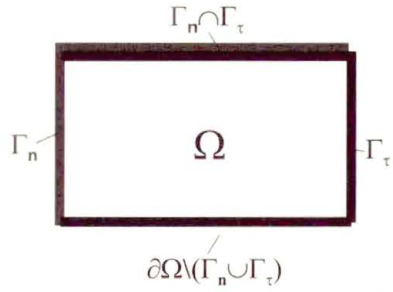

FIGURE 3. The boundary of computational domain—general settings

The following (essential) boundary conditions are postulated:

$$\begin{aligned} &\Gamma_n : \mathbf{u} \cdot \mathbf{n} = \xi(s), \\ &\Gamma_\tau : \mathbf{u} \times \mathbf{n} = \boldsymbol{\eta}(s). \end{aligned} \tag{1.11}$$

In other words, the normal component of the velocity field has a prescribed distribution at the part of the boundary Γ_n, while the tangent component (being actually equal to $\mathbf{n} \times \boldsymbol{\eta}(s)$) is given at Γ_τ. In general, there exists a nonempty product $\Gamma_n \cap \Gamma_\tau$, where full velocity vector is defined.

Since we are going to work with primitive variables (i.e. velocity and pressure), the following functional spaces are introduced:

- the velocity space

$$\mathbf{u} \in V = \left\{ \boldsymbol{v} \in \left[H^1(\Omega)\right]^3 : \boldsymbol{v} \times \boldsymbol{n} = 0 \text{ at } \Gamma_\tau, \quad \boldsymbol{v} \cdot \mathbf{n} = 0 \text{ at } \Gamma_n \right\},$$

  where H^1 denotes the first Sobolev space of functions which are square-integrable in Ω together with their partial derivatives of the first order
- the pressure space $p \in Q = L_0^2(\Omega)$ or $p \in Q = L^2(\Omega)$. Here, $L^2(\Omega)$ is the space of square-integrable functions in Ω, while $L_0^2(\Omega)$ is a linear subspace of $L^2(\Omega)$ containing functions which integral over the whole domain amounts to zero. Such normalization is necessary to avoid ambiguity of the pressure, which occurs if the boundary conditions are expressed in terms of purely kinematical quantities (velocity or vorticity).

The general variational form of the governing equation can be written as

$$\begin{aligned} (\partial_t \mathbf{u}, \boldsymbol{v}) + a(\mathbf{u}, \boldsymbol{v}) + b(\boldsymbol{v}, p) + c(\mathbf{u}, \mathbf{u}, \boldsymbol{v}) &= (\mathbf{f}, \boldsymbol{v}) + d(\boldsymbol{v}), \\ b(\mathbf{u}, q) = 0, \quad \boldsymbol{v} \in V, \quad q \in Q. \end{aligned} \tag{1.12}$$

In the above, the following notation has been used:

$$b(\boldsymbol{v}, p) = -\int_{\Omega} p\nabla \cdot \boldsymbol{v} d\mathbf{x} \text{ —pressure term,} \tag{1.13}$$

$$c(\mathbf{u}, \mathbf{u}, \boldsymbol{v}) = \int_{\Omega} \boldsymbol{v} \cdot \nabla \mathbf{u} \cdot \mathbf{u} d\mathbf{x} \text{ —convective term (nonlinear),} \tag{1.14}$$

$$(\mathbf{f}, \boldsymbol{v}) = \int_{\Omega} \mathbf{f} \cdot \boldsymbol{v} d\mathbf{x} \text{ —volume force term.} \tag{1.15}$$

The viscous term $a(\mathbf{u}, \mathbf{v})$ and the boundary term $d(\mathbf{v})$ depend on the form of the Navier-Stokes equation. Each of these forms generates a different form of the variational formulation and corresponding (natural) boundary conditions.

Consider first the "standard" form, where the viscous term in Navier-Stokes equation is expressed using the Laplacian of the velocity field

$$\rho\left(\partial_t \mathbf{u} + \nabla \mathbf{u} \cdot \mathbf{u}\right) = -\nabla p + \mu \Delta \mathbf{u} + \rho \mathbf{f}, \quad \nabla \cdot \mathbf{u} = 0. \tag{1.16}$$

We will refer to this form as the Form A. There is an instructive exercise to show that the viscous and boundary terms can be expressed as

$$a(\mathbf{u}, \boldsymbol{v}) = \mu \int_{\Omega} \nabla \mathbf{u} : \nabla \boldsymbol{v} d\mathbf{x}, \tag{1.17}$$

$$d(\boldsymbol{v}) = \int_{\partial\Omega \setminus \Gamma_n} \left[-p + \mu\left(\mathbf{n} \cdot \nabla \mathbf{u} \cdot \mathbf{n}\right)\right]\left(\boldsymbol{v} \cdot \mathbf{n}\right) ds + \int_{\partial\Omega \setminus \Gamma_\tau} \mu\left[\left(\nabla \mathbf{u} \cdot \mathbf{n}\right) \times \mathbf{n}\right] \cdot \left(\boldsymbol{v} \times \mathbf{n}\right) ds. \tag{1.18}$$

In order to obtain a solvable problem we have to prescribe the integrands in square brackets in the formula (1.18). In other words, we have to impose natural boundary conditions, namely

$$\begin{cases} -p + \mu\left(\mathbf{n} \cdot \nabla \mathbf{u} \cdot \mathbf{n}\right) = \xi(t, s) \text{ at } \partial\Omega \setminus \Gamma_n, \\ \mu\left[\left(\nabla \mathbf{u} \cdot \mathbf{n}\right) \times \mathbf{n}\right] = \boldsymbol{\eta}(t, s) \text{ at } \partial\Omega \setminus \Gamma_\tau. \end{cases} \tag{1.19}$$

Note that the quantities we define of the indicated portions of the boundary do not have any particular physical interpretation. One can think that for

that reason such approach is useless. However, we will show later that it is not a case. On the contrary—this formulation is a basis for some very useful generalization to be described later.

Final variational form of the Navier-Stokes equations can now be written as

$$\rho \int_{\Omega} (\partial_t \mathbf{u} + \nabla \mathbf{u} \cdot \mathbf{u}) \cdot \boldsymbol{v} d\mathbf{x} + \mu \int_{\Omega} \nabla \mathbf{u} : \nabla \boldsymbol{v} d\mathbf{x} - \int_{\Omega} p \nabla \cdot \boldsymbol{v} d\mathbf{x} = \rho \int_{\Omega} \mathbf{f} \cdot \boldsymbol{v} d\mathbf{x} + \int_{\Gamma \setminus \Gamma_n} \xi (\boldsymbol{v} \cdot \mathbf{n}) \, ds + \int_{\Gamma \setminus \Gamma_\tau} \boldsymbol{\eta} \cdot (\boldsymbol{v} \times \mathbf{n}) \, ds \quad (1.20)$$

For sufficiently regular solutions, this formulation implies that the boundary conditions (1.19) will be satisfied.

Consider now the form (to be referred to as the Form B) where the deformation rate tensor $\mathbf{D}$ appears directly in the viscous term of the momentum equation. This form of the governing equations, which is valid also for generalized Newtonian fluid, can be written as follows:

$$\rho (\partial_t \mathbf{u} + \nabla \mathbf{u} \cdot \mathbf{u}) = -\nabla p + 2\nabla \cdot (\mu \mathbf{D}_{\mathbf{u}}) + \rho \mathbf{f}, \quad \nabla \cdot \mathbf{u} = 0 \quad (1.21)$$

where $\mathbf{D}_{\mathbf{u}} = \frac{1}{2} \left(\nabla \mathbf{u} + \nabla^T \mathbf{u} \right)$ is the deformation rate tensor. Again, it left to the Reader as an exercise to show that the corresponding viscous and boundary terms are

$$a(\mathbf{u}, \boldsymbol{v}) = 2 \int_{\Omega} \mu \mathbf{D}_{\mathbf{u}} : \mathbf{D}_{\boldsymbol{v}} d\mathbf{x} \quad (1.22)$$

$$d(\boldsymbol{v}) = \int_{\partial\Omega \setminus \Gamma_n} [-p + 2\mu (\mathbf{n} \cdot \mathbf{D}_{\mathbf{u}} \cdot \mathbf{n})] (\boldsymbol{v} \cdot \mathbf{n}) \, ds + \int_{\partial\Omega \setminus \Gamma_\tau} 2\mu [(\mathbf{D}_{\mathbf{u}} \cdot \mathbf{n}) \times \mathbf{n}] \cdot (\boldsymbol{v} \times \mathbf{n}) \, ds. \quad (1.23)$$

Consequently, the natural boundary conditions to be imposed are

$$\begin{cases} \sigma_n \equiv -p + 2\mu (\mathbf{n} \cdot \mathbf{D}_{\mathbf{u}} \cdot \mathbf{n}) = \xi(t, s) \text{ at } \partial\Omega \setminus \Gamma_n, \\ \boldsymbol{\sigma}_\tau \equiv 2\mu [(\mathbf{D}_{\mathbf{u}} \cdot \mathbf{n}) \times \mathbf{n}] = \boldsymbol{\eta}(t, s) \text{ at } \partial\Omega \setminus \Gamma_\tau. \end{cases} \quad (1.24)$$

In contrast to the Form A (Eq. (1.16)), the above conditions have a straightforward interpretation: they simply define the boundary distributions of the

normal and/or the tangent component of the surface stress. They are often called the traction conditions.

The final variational form of the Navier-Stokes equation for this case reads

$$\rho \int_\Omega (\partial_t \mathbf{u} + \nabla \mathbf{u} \cdot \mathbf{u}) \cdot \boldsymbol{v} d\mathbf{x} + 2 \int_\Omega \mu \mathbf{D}_\mathbf{u} : \mathbf{D}_{\boldsymbol{v}} d\mathbf{x} - \int_\Omega p \nabla \cdot \boldsymbol{v} d\mathbf{x} = \rho \int_\Omega \mathbf{f} \cdot \boldsymbol{v} d\mathbf{x} + \int_{\partial\Omega \setminus \Gamma_n} \xi (\boldsymbol{v} \cdot \mathbf{n}) \, ds + \int_{\partial\Omega \setminus \Gamma_\tau} \boldsymbol{\eta} \cdot (\boldsymbol{v} \times \mathbf{n}) \, ds \quad (1.25)$$

Let us finally consider the third option—the Form C. This time the viscous term in the momentum equation is written using the curl operator and the vorticity field. We have

$$\rho (\partial_t \mathbf{u} + \nabla \mathbf{u} \cdot \mathbf{u}) = -\nabla p - \mu \nabla \times \boldsymbol{\omega} + \rho \mathbf{f}, \quad \nabla \cdot \mathbf{u} = 0 \quad (1.26)$$

where the vorticity field $\boldsymbol{\omega} = \nabla \times \mathbf{u}$ is used. The viscous and boundary terms for this case are expressed by the following formulae

$$a(\mathbf{u}, \boldsymbol{v}) = \mu \int_\Omega \boldsymbol{\omega} \cdot (\nabla \times \boldsymbol{v}) \, d\mathbf{x}, \quad (1.27)$$

$$d(\boldsymbol{v}) = -\int_{\partial\Omega \setminus \Gamma_n} p (\boldsymbol{v} \cdot \mathbf{n}) \, ds - \int_{\partial\Omega \setminus \Gamma_\tau} \mu [\mathbf{n} \times (\boldsymbol{\omega} \times \mathbf{n})] \cdot (\boldsymbol{v} \times \mathbf{n}) \, ds \quad (1.28)$$

and thus the corresponding natural boundary conditions are

$$\begin{cases} p = \xi(t, s) \text{ at } \partial\Omega \setminus \Gamma_n, \\ \mathbf{n} \times (\boldsymbol{\omega} \times \mathbf{n}) = \boldsymbol{\eta}(t, s) \text{ at } \partial\Omega \setminus \Gamma_\tau. \end{cases} \quad (1.29)$$

The physical interpretation is again direct: we need to define the boundary distribution of the static pressure and/or the tangent component of the vorticity field at the indicated parts of the boundary. Final variational form of the Navier-Stokes equation for this case is

$$\rho \int_\Omega (\partial_t \mathbf{u} + \nabla \mathbf{u} \cdot \mathbf{u}) \cdot \boldsymbol{v} d\mathbf{x} + \mu \int_\Omega (\nabla \times \mathbf{u}) \cdot (\nabla \times \boldsymbol{v}) \, d\mathbf{x} - \int_\Omega p \nabla \cdot \boldsymbol{v} d\mathbf{x} = \rho \int_\Omega \mathbf{f} \cdot \boldsymbol{v} d\mathbf{x} + \int_{\partial\Omega \setminus \Gamma_n} \xi (\boldsymbol{v} \cdot \mathbf{n}) \, ds + \int_{\partial\Omega \setminus \Gamma_\tau} \mu \boldsymbol{\eta} \cdot (\boldsymbol{v} \times \mathbf{n}) \, ds \quad (1.30)$$

1.3. Modeling Inlet/Outlet Condition in Cardiovascular Simulation

In this part of the notes we will briefly discus the problem of adequate selection of the inlet and outlet conditions in the cardiovascular simulations. We will assume that the flow domain has been "extracted" from the larger vessel system and therefore its boundary consists of the material part (walls of the vessels) and the inlet/outlet part. The latter is merely the effect of the "extraction" process—in principle, ideal inlet/outlet conditions should not impose any additional restrictions of the flow field.

Consider the repertoire of the boundary conditions described in the previous section from such point of view. Ideally, we would like to have full information about all components of the velocity vector at all inlets and outlets. If such information were available, all boundary conditions would be of the essential kind. Such situation, very desirable from the CFD viewpoint, is not realistic since detailed inlet/outlet velocity profiles (and their history in time!) cannot be measured at reasonable costs. Thus, we have to work with much less information about the flow field at inlet/outlet sections. Mathematically speaking: we have to resort some of the natural boundary conditions.

Some possible choices are:

- Setting one essential condition (typically, setting the tangent velocity to zero) and one natural condition, e.g. the static pressure or the normal stress. If I/O sections are sufficiently far away from bifurcations in the vessel system, the static pressure can be assumed uniform within each section and the section-averaged value obtained from simplified models (1D or lumped-parameter) can be used in full 3D simulations. Also, the normal stress is nearly uniform and does not differ much from the static pressure, because the viscosity-driven term is usually very small. Moreover—for flat I/O sections the surface-integral average of this term is zero.
- Setting two natural conditions. The advantage of such choice is that explicit setting of the tangent velocity (to zero) is avoided. Assumption of vanishing tangent velocity can be criticized for being not quite physical. Indeed, if a vortex structures appears in the flow domain, it will be convected towards some outlet section and it will inevitably generate nonzero tangent velocity while leaving the computational region. For

further purpose we will refer to this issue as a vortex-passage problem. We can also try to set both components of the surface stress, however, it is difficult to predict a reasonable distribution of the tangent stress. In particular, the tangent stress cannot be assumed to be zero since such choice is incompatible even with unidirectional flow fields of the Hagen-Poiseuille or Womersley flows.

The final conclusion is that none of the combinations of the boundary conditions are really satisfactory. The inlet/outlet conditions offered above are either too demanding (i.e. they require to excessive knowledge about the flow field) or too restrictive (i.e. the kinematical constrains implied by the conditions are likely to eliminate important physical effects from the simulation).

1.4. Deficient Boundary Conditions

In this section we discuss new approach to inlet/outlet conditions, which removes (at least partly) limitations of the classical repertoire of the boundary conditions described above, [12, 22, 24].

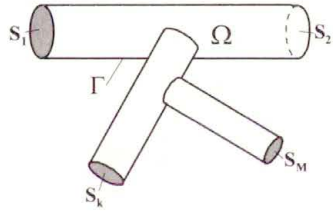

FIGURE 4. A system of branched vessels—geometry and notation

Consider again the computational domain modeling a selected part of the vessel system (see Fig. 4),

$$\Gamma_{\text{wall}} = \Gamma_n = \Gamma_\tau, \quad \Gamma_{\text{i/o}} = \bigcup_k S_k$$

$$\partial\Omega = \Gamma_{\text{wall}} \cup \Gamma_{\text{i/o}}$$

and the Form A (Eq. (1.16)) of the governing equations. We have already

shown that the corresponding boundary term is given as

$$d(\boldsymbol{v}) = \sum_k \int_{S_k} \left[-p + \mu\left(\mathbf{n}\cdot\nabla\mathbf{u}\cdot\mathbf{n}\right)\right]\left(\boldsymbol{v}\cdot\mathbf{n}\right) ds + \sum_k \int_{S_k} \mu\left[\left(\nabla\mathbf{u}\cdot\mathbf{n}\right)\times\mathbf{n}\right]\cdot\left(\boldsymbol{v}\times\mathbf{n}\right) ds.$$

Assume at the inlet/outlet sections S_k the following conditions:

$$\begin{aligned} p - \mu\left(\mathbf{n}\cdot\nabla\mathbf{u}\cdot\mathbf{n}\right) &= \Pi_k(t), \\ \left(\nabla\mathbf{u}\cdot\mathbf{n}\right)\times\mathbf{n} &= 0, \end{aligned} \tag{1.31}$$

where $k = 1, 2, \ldots, M$. Then, the boundary term reduces to the simple form

$$d(\boldsymbol{v}) = \sum_k \Pi_k(t)\Phi_k(\boldsymbol{v}), \tag{1.32}$$

where the functionals of the volumetric flow rate $\Phi_k(\boldsymbol{v}) = \int_{S_k} \boldsymbol{v}\cdot\mathbf{n}\, ds$ are introduced. The final variational form of the Navier-Stokes equations is

$$\rho\left(\partial_t\mathbf{v} + \nabla\mathbf{v}\cdot\mathbf{v}, \boldsymbol{v}\right) + \mu\left(\nabla\mathbf{v}, \nabla\boldsymbol{v}\right) - \left(p, \nabla\cdot\boldsymbol{v}\right) = \rho\left(\mathbf{f}, \boldsymbol{v}\right) - \sum_{k=1}^{M} \Pi_k(t)\Phi_k(\boldsymbol{v}) \tag{1.33}$$

A natural question arises about the physical interpretation of the functions $\Pi_k(t)$. We will show that, under certain geometric conditions, the functions $\Pi_k(t)$ describe the temporal variations of the section-averaged static pressure. Indeed, let us integrate the formula (1.31a) over the inlet/outlet section S_k

$$\int_{S_k} \left[p - \mu\left(\mathbf{n}\cdot\nabla\mathbf{u}\cdot\mathbf{n}\right)\right] ds = \Pi_k(t)\left|S_k\right|.$$

Assume next that S_k is a flat surface, i.e. the normal vector $\mathbf{n}$ is the same at all points of S_k. Then the following equality holds

$$\int_{S_k} \left(\mathbf{n}\cdot\nabla\mathbf{u}\cdot\mathbf{n}\right) d\sigma = 0. \tag{1.34}$$

Proof:

$\mathbf{n} = [1, 0, 0]$, $\quad \boldsymbol{\zeta} = [0, \zeta_2, \zeta_3]$ — normal vector at the flat contour ∂S_k,

$$\int_{S_k} \mathbf{n} \cdot \nabla \mathbf{u} \cdot \mathbf{n} = \int_{S_k} \partial_{x_1} u_1 dx_2 dx_3 = -\int_{S_k} (\partial_{x_2} u_2 + \partial_{x_3} u_3)\, dx_2 dx_3$$

$$= -\oint_{\partial S_k} (u_2 \zeta_2 + u_3 \zeta_3)\, dx_2 dx_3 = 0.$$

Thus, we conclude

$$\Pi_k(t) = \frac{1}{|S_k|} \int_{S_k} p ds$$

is a section-averaged pressure at S_k.

What is the meaning of the second boundary condition (1.31b)? Choosing the same geometric setting as in the aforementioned proof, it is immediate to show that this condition is equivalent to

$$\partial_{x_1} u_2 = \partial_{x_1} u_3 = 0. \tag{1.35}$$

Thus, the second condition is equivalent to the homogeneous Neumann condition formulated for the tangent velocity components. This condition seems to be better suited for the inlet/outlet modeling since no explicit restriction on the velocity itself is imposed. However, to the authors' best knowledge, the impact of this condition on the vortex-passage phenomenon has not yet been systematically studied.

The advantages of using deficient boundary conditions for inlets and outlets can be summarized as follows:

- Inlet/outlet section-average pressure is prescribed, but no particular surface distribution of the pressure field is explicitly assumed;
- There are no explicit restriction imposed on the normal or tangent velocity distributions;
- Additional kinematic constrains can be incorporated in the formulation of the flow problem. For instance, we can specify the time variation of the volumetric flow rate through a given inlet/outlet. In such case, the section-averaged pressure $\Pi_k(t)$ corresponding to this inlet/outlet works as the Lagrange multiplier, which is a priori unknown and has to be determined in the solution process.

2. Numerical Simulation of Nonstationary Laminar Flows in a Pipe System Using Spectral Elements

In this part of the lecture we present a particular simulation method based on the usage of deficient boundary conditions, spectral element approximations in space and the OIFS[1)] time integration scheme. We describe main ingredients of the method as well as selected algorithms, which are essential for numerical efficiency. More detailed exposition can be found in the paper [17].

2.1. Introduction

The objectives are to develop a complete computational method and its efficient implementation to perform computer simulations of nonstationary flows in complex vessel systems. The test example for the solver is the simplified model of the modified Blalock-Taussig shunt, which will be described in more details in the Part 3 of these notes.

The numerical method described in this chapter can be considered the first stage of development of the future numerical package for cardiovascular simulations. Therefore, the following assumption have been made

- Time-independent geometry of the computational domain;
- Newtonian liquid model of blood rheology;
- Inlet/outlet conditions should be formulated in terms of "easily" measurable or estimable (integral) quantities: section-averaged static pressure or volumetric flow rates. Various combinations of such conditions should be possible.
- Application of the high-order spatial approximation with hexahedral spectral elements;
- Application of higher-order time-integration schemes.

2.2. Formulation of the Flow Problem

The computational domain and be presented schematically as in Fig. 5

Γ — solid boundary of the flow domain Ω,

S_k — inlet/outlet sections (k=1,..,N).

[1)] OIFS—Operator-Integration-Factor Splitting

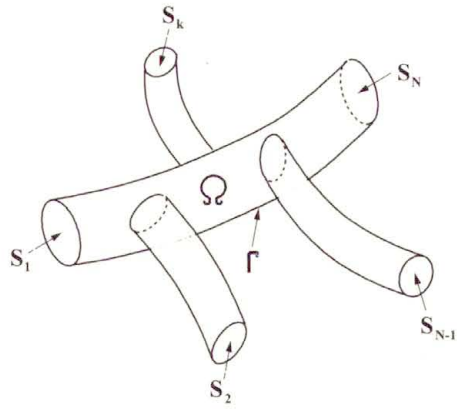

FIGURE 5. Computational domain

Governing equations are

$$\begin{cases} \rho\left(\partial_t \mathbf{v} + \nabla \mathbf{v} \cdot \mathbf{v}\right) = -\nabla p + \mu \nabla^2 \mathbf{v}, \\ \nabla \cdot \mathbf{v} = 0 \end{cases} \tag{2.1}$$

and the boundary conditions are defined as follows:

- Material boundary:

$$\Gamma : \mathbf{v}|_\Gamma = \mathbf{0}, \tag{2.2}$$

- Inlet/outlet conditions:
  - VF-type

$$\Phi_i(\mathbf{v}) \equiv \int_{S_i} \mathbf{v} \cdot \mathbf{n} ds = F_i(t), \quad i = 1, \ldots, N_{\mathrm{VF}}, \tag{2.3}$$

  - AP-type

$$\frac{1}{|S_{N_{\mathrm{VF}}+i}|} \int_{S_{N_{\mathrm{VF}}+i}} p ds = P_i(t), \quad i = 1, \ldots, N_{\mathrm{AP}}. \tag{2.4}$$

The variational formulation is stated as follows:

Find:

$$\mathbf{v} \in V = \{\mathbf{v} \in [H^1(\Omega)]^3 : \mathbf{v}|_\Gamma = 0\},$$
$$p \in Q = L^2(\Omega),$$
$$\lambda_i(t) \in R, \quad i = 1, \ldots, N_{\mathrm{VF}} \text{ (Lagrange multipliers)},$$

such that

$$\rho(\partial_t \mathbf{v} + \nabla \mathbf{v} \cdot \mathbf{v}, \boldsymbol{v}) + \mu(\nabla \mathbf{v}, \nabla \boldsymbol{v}) + \sum_{i=1}^{N_{\mathrm{VF}}} \lambda_i \Phi_i(\boldsymbol{v}) + \sum_{i=1}^{N_{\mathrm{AP}}} P_i(t)\, \Phi_{N_{VF}+i}(\boldsymbol{v}) - (p, \nabla \cdot \boldsymbol{v}) = 0,$$

$$(q, \nabla \cdot \mathbf{v}) = 0 \quad \forall \boldsymbol{v} \in V, \quad \forall q \in Q,$$

and

$$\Phi_i(\mathbf{v}) = F_i(t), \quad i = 1, \ldots, N_{\mathrm{VF}}.$$
$$\mathbf{v}|_{t=t_0} = \mathbf{v}_0 \quad \text{— initial condition}$$

It follows from the Sec. 1.4 that the classical boundary conditions corresponding to the above formulation are

$$\begin{cases} p - \mu(\mathbf{n} \cdot \nabla \mathbf{u} \cdot \mathbf{n}) = P_k \text{ at } S_k, & k = 1, \ldots, N_{\mathrm{AP}}, \\ p - \mu(\mathbf{n} \cdot \nabla \mathbf{u} \cdot \mathbf{n}) = \lambda_k \text{ at } S_k, & k = N_{AP} + 1, \ldots, N_{\mathrm{AP}} + N_{\mathrm{VF}}, \\ (\nabla \mathbf{u} \cdot \mathbf{n}) \times \mathbf{n} = 0 \text{ at } S_k, & k = 1, \ldots, N_{\mathrm{AP}} + N_{\mathrm{VF}}. \end{cases} \tag{2.5}$$

It has been also shown already that the physical interpretation of $P_k(t)$ (given functions) and $\lambda_k(t)$ (to be evaluated) is the section-averaged static pressure.

2.3. Time Integration Schemes

In order to develop accurate yet computationally efficient numerical method one has to care about the choice of appropriate time integration scheme. Here we discuss shortly some possibilities. To make our discussion simpler, we will consider a model initial-value problem

$$\begin{cases} u'(t) = \underbrace{Lu}_{\text{linear term}} + \underbrace{N(u)u}_{\text{nonlinear term}} + \underbrace{f}_{\text{forcing term}}, \\ u(0) = u_0. \end{cases} \tag{2.6}$$

In the context of the incompressible flow simulation, the reasonable choice is to apply the stiff-stable backward-differentiation formulae (BDF). In general, the K-order BDF method can be written in the form of

$$\beta_0 u^{(n+1)} - \sum_{k=1}^{K} \beta_k u^{(n+1-k)} = \Delta t \left[L u^{(n+1)} + N(u^{(n+1)}) u^{(n+1)} + f^{(n+1)} \right] \tag{2.7}$$

The coefficients of the BDF methods of different order have been summarized in the Table 1.

TABLE 1.

K	β_0	β_1	β_2	β_3	β_4
1	1	1	—	—	—
2	3/2	2	−1/2	—	—
3	11/6	3	−3/2	1/3	—
4	25/12	4	−3	4/3	−1/4

The BDF methods are implicit and thus unconditionally stable. On the other hand, the nonlinear boundary-value problem has to be solved at each time step, which is computationally very demanding, especially in the context of the CFD. It is desirable to avoid solving a huge nonlinear problem at each time step, even though the unconditional stability will be lost. A number of different approaches can be proposed, like:

(A) Extrapolation of the nonlinear term (of the same order as BDF), see [7, 13, 19]. The nonlinear term in extrapolated from its values at previous time steps as follows

$$N^{(n+1)} \approx \sum_{k=1}^{K} \alpha_k N^{(n+1-k)}, \qquad N^{(n+1-k)} \equiv N(u^{(n+1-k)}) u^{(n+1-k)}, \quad k = 0, 1, \ldots, K. \tag{2.8}$$

TABLE 2.

K	α_1	α_2	α_3	α_4
1	1	—	—	—
2	2	−1	—	—
3	3	−3	1	—
4	4	−6	4	−1

Table 2 contains the coefficients of the extrapolation methods of different order. In the CFD application, the Stokes problem has to be solved at each time step of the flow simulation.

(B) Linearization of the nonlinear term based on the velocity extrapolation [7, 23].
More sophisticated approach consists of extrapolating the velocity that appears in the algebraic way, while these parts of the nonlinear term where the velocity id differentiated remain in the original implicit form.

$$N(u^{(n+1)})u^{(n+1)} \to N(u_*)u^{(n+1)}, \quad u_* = \sum_{k=1}^{K} \alpha_k u^{(n+1-k)}. \tag{2.9}$$

This way we obtain linear approximation of the nonlinear term, which in the CFD applications leads to the Oseen problem to be solved at each time step. The latter problem is more difficult to solve that the Stokes problem, but the method will posses better stability properties.

(C) Operator-Integration-Factor-Splitting Methods [7, 10, 14, 17, 19].
This method is based on the idea of the operator splitting. At each time step the following linear problem has to be solved

$$\beta_0 u^{(n+1)} - \sum_{k=1}^{K} \beta_k \hat{u}_k^{(n+1)} = \Delta t L u^{(n+1)}, \tag{2.10}$$

$$\hat{u}_k^{(m+1)} \equiv \hat{u}_k(t_{n+1}),$$

where $\hat{u}_k$ are defined as the solutions to the following initial value problems

$$\begin{cases} \dfrac{d}{dt}\hat{u}_k = N(\hat{u}_k)\hat{u}_k, \\ \hat{u}_k(t_{n+1-k}) = u^{(n+1-k)}. \end{cases} \tag{2.11}$$

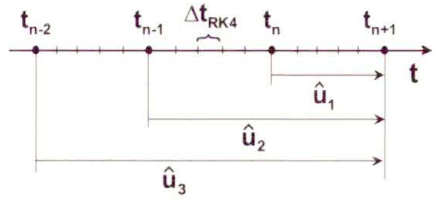

FIGURE 6. The OIFS method—more details in text

The initial-value problems are solved numerically with any higher order explicit method, which behaves well for purely convective problems (4-order Runge-Kutta, Taylor-Galerkin methods). The integration step is chosen as $\Delta t_{\mathrm{RK4}} = \Delta t/M$, where typically $M \leq 5$. The overall order of accuracy is equal to the minimum of the number K and the order of the method used for the systems (2.11).

2.4. Finite Dimensional Approximation

Whichever time discretization method is used, a boundary value problem for partial differential equations is obtained at each simulation step. In order to obtain approximate solution, the following basic fields in the velocity space V are introduced

$$\begin{aligned}
&\boldsymbol{v}_1 = [w_1, 0, 0],\ \boldsymbol{v}_2 = [w_2, 0, 0], \ldots,\ \boldsymbol{v}_{N_V} = [w_{N_\mathrm{V}}, 0, 0],\\
&\boldsymbol{v}_{N_V+1} = [0, w_1, 0],\ \boldsymbol{v}_{N_\mathrm{V}+2} = [0, w_2, 0], \ldots,\ \boldsymbol{v}_{2N_\mathrm{V}} = [0, w_{N_\mathrm{V}}, 0],\\
&\boldsymbol{v}_{2N_\mathrm{V}+1} = [0, 0, w_1],\ \boldsymbol{v}_{2N_\mathrm{V}+2} = [0, 0, w_2], \ldots,\ \boldsymbol{v}_{3N_\mathrm{V}} = [0, 0, w_{N_\mathrm{V}}].
\end{aligned} \tag{2.12}$$

The velocity field at a given time instant is approximated by the linear combination of the basic fields

$$\mathbf{v}^{(m+1)} = \sum_{j=1}^{N_V} \left(\mathbf{u}_1^{(m+1)}\right)_j \boldsymbol{v}_j + \sum_{j=1}^{N_V} \left(\mathbf{u}_2^{(m+1)}\right)_j \boldsymbol{v}_{N_V+j} + \sum_{j=1}^{N_V} \left(\mathbf{u}_3^{(m+1)}\right)_j \boldsymbol{v}_{2N_V+j} \tag{2.13}$$

Analogously, the basic function $\{q_j\}$ in the Q are introduced and the pressure approximation is defined as

$$p^{(m+1)} = \sum_{j=1}^{N_Q} \left(\boldsymbol{\pi}^{(m+1)}\right)_j q_j. \tag{2.14}$$

Hence, at each time instant $3N_\mathrm{V} + N_\mathrm{Q}$ coefficients, which represent the instantaneous velocity and pressure fields, have to be computed.

It can be shown that in the effect the discretization procedure the following algebraic structures are obtained

$$
\begin{aligned}
(\mathbf{M}_V)_{ij} &= (w_i, w_j) \equiv \int_\Omega w_i w_j d\mathbf{x} && \text{— mass matrix,}\\
(\mathbf{K}_V)_{ij} &= (\nabla w_i, \nabla w_j) \equiv \int_\Omega \nabla w_i \cdot \nabla w_j d\mathbf{x} && \text{— Laplace (“stiffness”) matrix,}\\
\mathbf{A} &= \frac{\beta_0}{\Delta t}\mathbf{M}_V + \nu \mathbf{K}_V && \text{— Helmholtz matrix,}\\
(\mathbf{D}_\alpha)_{ij} &= -(q_i, \partial_{X_\alpha} w_j), \quad \alpha = 1,2,3, && \text{— divergence/gradient matrices,}\\
\left(\mathbf{\Lambda}^{\mathbf{F}}_\alpha\right)_{ij} &= \Phi_i(\boldsymbol{v}_j), \quad i = 1,\ldots,N_{\mathrm{VF}},\\
\left(\mathbf{\Lambda}^{\mathbf{P}}_\alpha\right)_{ij} &= \Phi_{N_F+i}(\boldsymbol{v}_j), \quad i = 1,\ldots,N_{\mathrm{AP}}, && \text{— I/O volumetric flux matrices}\\
j &= (\alpha-1)N_{\mathrm{V}}+1,\ldots,\alpha N_{\mathrm{V}}, \quad \alpha = 1,2,3.\\
\left(\mathbf{r}^{(m+1)}_\alpha\right)_i &= -\frac{1}{\Delta t}\sum_{k=1}^{K}\beta_k\left((\hat{\mathbf{v}}^{(m+1)}_k)_\alpha, w_i\right), && \text{— r-h-s vector}\\
i &= 1,\ldots,N_{\mathrm{V}}, \quad \alpha = 1,2,3.
\end{aligned}
\tag{2.15}
$$

2.5. Spectral Element Method

In this section we describe briefly the main features of the spectral element discretization using hexahedral elements and the nodal (or collocation) approach. The computational domain is meshed with hexahedral cells. Each cell can be mapped into the standard cube $[-1,1]^3$ where all differentiation and integration operations are carried out.

The mapping from a physical element to the standard cube can be defined in different forms dependently on the geometrical information included. In

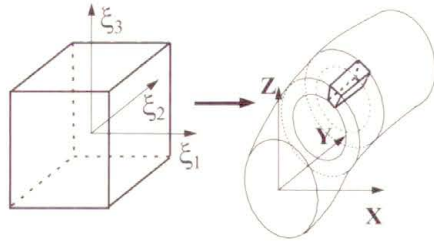

FIGURE 7. The standard cube and physical element

the simplest variant, the vertex-based transformation of the standard cube to a physical element can be written as follows

$$\begin{aligned}\mathbf{x}(\xi_1,\xi_2,\xi_3) &= \frac{1}{8}(1-\xi_1)(1-\xi_2)(1-\xi_3)\,\mathbf{x}_1 + \frac{1}{8}(1+\xi_1)(1-\xi_2)(1-\xi_3)\,\mathbf{x}_2 \\ &+ \frac{1}{8}(1+\xi_1)(1+\xi_2)(1-\xi_3)\,\mathbf{x}_3 + \frac{1}{8}(1-\xi_1)(1+\xi_2)(1-\xi_3)\,\mathbf{x}_4 \\ &+ \frac{1}{8}(1-\xi_1)(1-\xi_2)(1+\xi_3)\,\mathbf{x}_5 + \frac{1}{8}(1+\xi_1)(1-\xi_2)(1+\xi_3)\,\mathbf{x}_6 \\ &+ \frac{1}{8}(1+\xi_1)(1+\xi_2)(1+\xi_3)\,\mathbf{x}_7 + \frac{1}{8}(1-\xi_1)(1+\xi_2)(1+\xi_3)\,\mathbf{x}_8 \end{aligned} \tag{2.16}$$

More sophisticated curvilinear transformations are also possible—the practical implementations are usually based on the Gordon-Hall blending procedure (see for instance [7], pp.183-184).

Each cell of the grid is equipped with the pair of internal collocation meshes, which are the transformation images of the two standard collocation grid in the cube $[-1,1]^3$: one for the velocity and another one for the pressure. The standard velocity collocation mesh is constructed as follows

$$\begin{gathered}\xi_V^{(0)} = -1, \quad \xi_V^{(M_V-1)} = 1, \\ \left\{\xi_V^{(j)}, \quad j = 1,\ldots,M_V-2\right\} \quad \text{— roots of the Jacobi pol. } P^{1,1}_{M_V-2}.\end{gathered} \tag{2.17}$$

and the corresponding local basic functions in $[-1,1]^3$ are defined as

$$b^V_{ijk}(\xi_1,\xi_2,\xi_3) = L^V_i(\xi_1)L^V_j(\xi_2)L^V_k(\xi_3), \quad i,j,k = 0,\ldots,M_V-1 \tag{2.18}$$

where $L^V_i(\xi_V^{(j)}) = \delta^j_i$, $(j = 0,\ldots,M_V-1)$ are the Lagrange interpolating polynomials corresponding to the nodes (2.17).

The pressure collocation nodes are constructed in the similar manner:

$$\{\xi_P^{(j)}, \quad j = 0,\ldots,M_P-1\} \quad \text{— roots of the Legendre pol. } P_{M_P-1}. \tag{2.19}$$

The local basic pressure functions are then defined in the following form

$$b^P_{ijk}(\xi_1,\xi_2,\xi_3) = L^P_i(\xi_1)L^P_j(\xi_2)L^P_k(\xi_3), \quad i,j,k = 0,\ldots,M_P-1 \tag{2.20}$$

where $L^P_i(\xi_P^{(j)}) = \delta^j_i$, $(j = 0,\ldots,M_P-1)$ are the Lagrange's interpolating polynomials corresponding to the nodes (2.19).

Since detailed expositions of the spectral element approach can be found in several recent handbooks and monographs [3, 4, 6, 7], we will merely summarize some basic features of this approach:

- Straightforward interpretation of the coefficients of the velocity and pressure expansions with respect to the local basic functions—the coefficients are simply the values of velocity or pressure at the corresponding collocation nodes.
- Differentiation: local velocity representations are differentiated inside the standard element and the derivatives are re-interpolated on the collocation mesh (the pseudo-spectral approach). Next, the derivatives with respect to physical coordinates are computed with the use of the (inverse) Jacobi matrices.
- Volume and surface integrals are calculated with the use of Gauss-Jacobi-Lobatto and Gauss-Legendre formulae based on the velocity and pressure collocation meshes, respectively.
- The local basic functions are L^2-orthogonal with respect to the Gauss integration. Consequently, the mass matrix $\mathbf{M}_{\mathrm{V}}$ (also the pressure mass matrix $\mathbf{M}_{\mathrm{P}}$ used in a preconditioner of the conjugate gradient iterations) is purely diagonal.
- Div-stability condition (necessary for the Stokes matrix be invertible) is fulfilled when $N_V \geq N_P + 2$.

2.6. Summary of the Computational Method

In this section we give a brief description of the OIFS-based spectral element method using hexahedral grids. The numerical problem involves computation of the velocity and pressure fields as well as the Lagrange multipliers (section-averaged pressures at VF-type inlets/outlets). Superposition of special Stokes solutions is used to construct the full solution at each time instant.

A. Preparatory stage (time-independent space discretization and fixed Δt)

The following Stokes problems are solved

$$\begin{bmatrix} \mathbf{A} & \mathbf{0} & \mathbf{0} & (\mathbf{D}_1)^{\mathrm{T}} \\ \mathbf{0} & \mathbf{A} & \mathbf{0} & (\mathbf{D}_2)^{\mathrm{T}} \\ \mathbf{0} & \mathbf{0} & \mathbf{A} & (\mathbf{D}_3)^{\mathrm{T}} \\ \mathbf{D}_1 & \mathbf{D}_2 & \mathbf{D}_3 & \mathbf{0} \end{bmatrix} \begin{bmatrix} \mathbf{u}_1^{\{\mathbf{k}\}} \\ \mathbf{u}_2^{\{\mathbf{k}\}} \\ \mathbf{u}_3^{\{\mathbf{k}\}} \\ \pi^{\{\mathbf{k}\}} \end{bmatrix} = \begin{bmatrix} -\left(\mathbf{\Lambda}_1^F\right)^{\mathrm{T}} \mathbf{e}^{\{k\}} \\ -\left(\mathbf{\Lambda}_2^F\right)^{\mathrm{T}} \mathbf{e}^{\{k\}} \\ -\left(\mathbf{\Lambda}_3^F\right)^{\mathrm{T}} \mathbf{e}^{\{k\}} \\ \mathbf{0} \end{bmatrix}, \tag{2.21}$$

where

$$e_j^{\{k\}} = \begin{cases} 0 \text{ if } j \neq k, \\ 1 \text{ if } j = k. \end{cases}$$

Then, the following array is created

$$\mathbf{T_F} = \begin{bmatrix} f_1^{\{1\}} & \cdots & f_1^{\{N_{\mathrm{VF}}\}} \\ \vdots & \vdots & \vdots \\ f_{N_{\mathrm{VF}}}^{\{1\}} & \cdots & f_{N_{\mathrm{VF}}}^{\{N_{\mathrm{VF}}\}} \end{bmatrix}, \tag{2.22}$$

where

$$f_j^{\{k\}} = \left(\sum_{\alpha=1}^{3} \mathbf{\Lambda}_\alpha^F \mathbf{u}_\alpha^{\{k\}} \right)_j, \quad j = 1, \ldots, N_{\mathrm{VF}}. \tag{2.23}$$

If the flow domain and grid geometry as well as the time integration steps are fixed, the above solutions are computed once and forever.

B. Main simulation stage

The computational procedure to update the solution at $t = t_n$ to $t = t_{n+1}$ consists of the following steps:

1. Integration of convective terms (K-steps OIFS)

$$\begin{gathered} \frac{d}{dt} \left(\hat{\mathbf{u}}_\alpha \right)_k = -C_\alpha \left[\left(\hat{\mathbf{u}}_1 \right)_k, \left(\hat{\mathbf{u}}_2 \right)_k, \left(\hat{\mathbf{u}}_3 \right)_k \right] \left(\hat{\mathbf{u}}_\alpha \right)_k, \quad \alpha = 1, 2, 3. \\ \left(\hat{\mathbf{u}}_\alpha \right)_k \left(t = t^{(m-k+1)} \right) = \mathbf{u}_\alpha^{(m-k+1)}, \quad k = 1, \ldots, K. \end{gathered} \tag{2.24}$$

Numerical integration: 4^{th} order Runge-Kutta method with the sub-step $\Delta t / M_S$ up to the time instant $t^{(m+1)} = t^{(m)} + \Delta t$. As a result we get

$$\left(\hat{\mathbf{u}}_\alpha \right)_k^{(m+1)} = \left(\hat{\mathbf{u}}_\alpha \right)_k \left(t = t^{(m+1)} \right), \quad \alpha = 1, 2, 3, \quad k = 1, \ldots, K. \tag{2.25}$$

2. Solution of the reduced Stokes problem

$$\begin{bmatrix} \mathbf{A} & \mathbf{0} & \mathbf{0} & (\mathbf{D}_1)^{\mathrm{T}} \\ \mathbf{0} & \mathbf{A} & \mathbf{0} & (\mathbf{D}_2)^{\mathrm{T}} \\ \mathbf{0} & \mathbf{0} & \mathbf{A} & (\mathbf{D}_3)^{\mathrm{T}} \\ \mathbf{D}_1 & \mathbf{D}_2 & \mathbf{D}_3 & \mathbf{0} \end{bmatrix} \begin{bmatrix} \mathbf{u}_1^{\{0\}} \\ \mathbf{u}_2^{\{0\}} \\ \mathbf{u}_3^{\{0\}} \\ \boldsymbol{\pi}^{\{0\}} \end{bmatrix}^{(m+1)} = \begin{bmatrix} \mathbf{r}_1 \\ \mathbf{r}_2 \\ \mathbf{r}_3 \\ \mathbf{0} \end{bmatrix}^{(m+1)}, \tag{2.26}$$

where

$$\mathbf{r}_\alpha^{(m+1)} = -\frac{1}{\Delta t}\sum_{k=1}^{K}\beta_k \mathbf{M}_\mathbf{V}(\hat{\mathbf{u}}_\alpha)_k^{(m+1)} - \left(\mathbf{\Lambda}_\alpha^P\right)^{\mathrm{T}}\mathbf{P}^{(m+1)}, \quad \alpha = 1,2,3. \tag{2.27}$$

Solution procedure consists in the following 3 steps

(i)

$$\mathbf{A}\,\tilde{\mathbf{u}}_\alpha = \mathbf{r}_\alpha^{(m+1)} - \mathbf{D}_\alpha^{\mathrm{T}}\boldsymbol{\pi}^{\{0\}(m)}, \quad \alpha = 1,2,3. \tag{2.28}$$

(ii)

$$\mathbf{S}\boldsymbol{\pi}' = \sum_{\alpha=1}^{3}\mathbf{D}_\alpha\tilde{\mathbf{u}}_\alpha, \quad \mathbf{S} = \sum_{\alpha=1}^{3}\mathbf{D}_\alpha\mathbf{A}^{-1}\mathbf{D}_\alpha^{\mathrm{T}},$$
$$\boldsymbol{\pi}^{\{0\}(m+1)} = \boldsymbol{\pi}^{\{0\}(m)} + \boldsymbol{\pi}', \tag{2.29}$$

(iii)

$$\mathbf{A}\mathbf{u}'_\alpha = -\mathbf{D}_\alpha^{\mathrm{T}}\boldsymbol{\pi}', \quad \mathbf{u}_\alpha^{\{0\}(m+1)} = \mathbf{u}_\alpha^{\{0\}(m)} + \mathbf{u}'_\alpha, \quad \alpha = 1,2,3. \tag{2.30}$$

3. Determination of the Lagrange multipliers

The following linear system containing N_{VF} equations is solved

$$\mathbf{T}_\mathbf{F}\boldsymbol{\lambda}^{(m+1)} = \mathbf{F}^{(m+1)} - \sum_{\alpha=1}^{3}\mathbf{\Lambda}_\alpha^F\mathbf{u}_\alpha^{\{0\}(m+1)}. \tag{2.31}$$

The physical interpretation of the computed multipliers: the section-averaged static pressure at VF-type inlets/outlets, at the time $t = t_{n+1}$.

4. Computing the final form of the solution at the time $t = t_{n+1}$

The final solution is constructed as the linear combination of the Stokes solutions

$$\begin{Bmatrix} \mathbf{u}_1^{(m+1)} \\ \mathbf{u}_2^{(m+1)} \\ \mathbf{u}_3^{(m+1)} \\ \boldsymbol{\pi}^{(m+1)} \end{Bmatrix} = \begin{Bmatrix} \mathbf{u}_1^{\{0\}(m+1)} \\ \mathbf{u}_2^{\{0\}(m+1)} \\ \mathbf{u}_3^{\{0\}(m+1)} \\ \boldsymbol{\pi}^{\{0\}(m+1)} \end{Bmatrix} + \sum_{k=1}^{N_{\mathrm{VF}}}\lambda_k^{(m+1)} \begin{Bmatrix} \mathbf{u}_1^{\{k\}} \\ \mathbf{u}_2^{\{k\}} \\ \mathbf{u}_3^{\{k\}} \\ \boldsymbol{\pi}^{\{k\}} \end{Bmatrix} \tag{2.32}$$

2.7. Selected Numerical Algorithms

2.7.1. Preconditioned conjugate gradients (PCG). The PCG method [8] is used to solve linear systems with the Helmholtz and Uzawa matrices (both are SPD-symmetric and positive definite). Here is the summary of this algorithms for the SPD system $\mathbf{Sx} = \mathbf{b}$.

Start: $\mathbf{x}^{(0)}$; $\mathbf{r}^{(0)} = \mathbf{b} - \mathbf{Sx}^{(0)}$; solve $\mathbf{P}\tilde{\mathbf{r}}^{(0)} = \mathbf{r}^{(0)}$; $\mathbf{p}^{(0)} = \tilde{\mathbf{r}}^{(0)}$.

For k = 1,2,...:

(i) $\alpha_k = -\left(\tilde{\mathbf{r}}^{(k)}, \mathbf{r}^{(k)}\right) / \left(\mathbf{p}^{(k)}, \mathbf{Sp}^{(k)}\right)$,

(ii) $\mathbf{x}^{(k+1)} = \mathbf{x}^{(k)} - \alpha_k \mathbf{p}^{(k)}$

(iii) $\mathbf{r}^{(k+1)} = \mathbf{r}^{(k)} + \alpha_k \mathbf{Sp}^{(k)}$ $\quad \rightarrow$ convergence test $\left\| r^{(k+1)} \right\| / \|b\| < \varepsilon$,

(iv) solve $\mathbf{P}\tilde{\mathbf{r}}^{(k+1)} = \mathbf{r}^{(k+1)}$,

(v) $\beta_k = \left(\tilde{\mathbf{r}}^{(k+1)}, \mathbf{r}^{(k+1)}\right) / \left(\tilde{\mathbf{r}}^{(k)}, \mathbf{r}^{(k)}\right)$,

(vi) $\mathbf{p}^{(k+1)} = \tilde{\mathbf{r}}^{(k+1)} + \beta_k \mathbf{p}^{(k)}$.

The Helmholtz system can be efficiently preconditioned by the diagonal matrix

$$\mathbf{P} = \operatorname{diag}\{\frac{\beta_0}{\Delta t}\mathbf{M_V} + \mu\mathbf{K}\}.$$

Fast computation of the pressure correction is much more tricky!

2.7.2. Preconditioning in the pressure solver. The overall performance of the Navier-Stokes solver depends mostly on the efficiency of the pressure determination. The corresponding algebraic problem is defined as follows

$$\mathbf{S}\pi' = \sum_{\alpha=1}^{3} \mathbf{D}_\alpha \tilde{\mathbf{u}}_\alpha, \quad \mathbf{S} = \sum_{\alpha=1}^{3} \mathbf{D}_\alpha \mathbf{A}^{-1} \mathbf{D}_\alpha^T, \tag{2.33}$$

where

$$\mathbf{A} = \frac{\beta_0}{\Delta t}\mathbf{M}_V + \mu\mathbf{K}_V.$$

It has been demonstrated [9, 15] that appropriate preconditioning matrix for this problem (suitable for both low and higher Reynolds numbers) can be constructed in the following form

$$\mathbf{P}^{-1} = \nu\mathbf{M}_\mathbf{P}^{-1} + \frac{\beta_0}{\Delta t}\mathbf{E}^{-1}, \tag{2.34}$$

where

$$\mathbf{E} = \sum_{k=1}^{3} \mathbf{D}_k \mathbf{M}_\mathbf{V}^{-1} \mathbf{D}_k^{\mathrm{T}}$$

and $\mathbf{M}_P$ denotes the pressure mass matrix (diagonal). We still need an efficient method for solving internally (i.e., at each iteration of the PCG method) the system with the matrix $\mathbf{E}$, which itself is poorly conditioned.

2.7.3. Solution of Eq = r. This section is based upon the references [10, 16, 17, 19]; we shall use the following notation:

N_P — number of the pressure collocation nodes in each spectral element

K — number of the spectral elements in the flow domain

$N = \dim E = N_\mathrm{P} \cdot K$ — global number of the pressure nodes

Consider the rectangular matrix $\mathbf{J}$, where $\dim(\mathbf{J}) = (N, K)$, such that:

- each column of $\mathbf{J}$ has a structure of K blocks with N_P entries,
- in k-th column all blocks are zero except the k-th block, which is filled with 1's.

Thus, the columns of the matrix $\mathbf{J}$ are the orthonormal vectors in R^N and $\mathbf{J}^{\mathrm{T}}\mathbf{J} = \mathbf{I}$. Next, the K-dimensional subspace

$$\Pi = \left\{ \boldsymbol{\pi} \in R^N : \boldsymbol{\pi} = \mathbf{J}\mathbf{u},\ \mathbf{u} \in R^K \right\} \text{ in } R^N$$

is introduced. Conceptually, the space Π contains representations of piecewise constant fields in the computational domain, i.e. such fields which are uniformly distributed within each individual spectral element.

The solution is sought in the form of the sum of the piecewise constant "background" and the "correction" belonging to the orthogonal space $\Pi^\perp$

$$\mathbf{q} = \mathbf{J}\mathbf{q}_0 + \mathbf{q}_1, \quad \mathbf{q}_0 \in \mathbf{R}^K. \tag{2.35}$$

Projection operator on $\Pi^\perp$ along $E(\Pi)$ is introduced as

$$\mathbf{P}_{\Pi^\perp} = \mathbf{I} - \mathbf{E}\mathbf{J}\mathbf{E}_0^{-1}\mathbf{J}^{\mathrm{T}}, \tag{2.36}$$

where $\mathbf{E}_0 = \mathbf{J}^T\mathbf{E}\mathbf{J}$. Then, the vector $\mathbf{q}_1$ is determined as the (unique) element from $\Pi^\perp$ satisfying the following linear system

$$\mathbf{H}\mathbf{q}_1 = \mathbf{P}_{\Pi^\perp}\mathbf{r}, \quad \mathbf{H} = \mathbf{P}_{\Pi^\perp}\mathbf{E}. \tag{2.37}$$

The linear system (2.34) is solved using PCG iterations with the block $\{E\}$ preconditioner [10, 19]. The efficient way to deal with the local systems for each individual element is to use the method of fast diagonalization. The vector $\mathbf{q}_0$ is determined from the following SPD system containing K equations, solved by the noniterative method (e.g., the Compressed-Sparse-Row-based Choleski solver)

$$\mathbf{E}_0\mathbf{q}_0 = \mathbf{J}^{\mathrm{T}}\left(\mathbf{r} - \mathbf{E}\mathbf{q}_1\right) \tag{2.38}$$

The computational performance of the pressure solver preconditioning (Pentium IV 2.6 GHz, 512 KB cache, 512 MB RAM), where $K = 1536$, $N = 5$, $\varepsilon = 10^{-10}$ has been summarized in the Table 3.

TABLE 3. Performance of pressure solver

M_{INT}	0	5	10	12	15	18	20
M	420	39	22	18	15	13	13
Time [s]	1398.8	198.5	150.9	136.3	129.1	125.8	134.9
Acceler.	1	7	9.3	10.3	10.8	11.1	10.4

M_{INT} denotes the number of internal PCG iterations for the linear system with the matrix $\mathbf{H}$ and M is the number of PCG iterations of the pressure solver.

2.7.4. Efficient solution of long sequences of large linear systems with the same SPD matrix. The overall computational performance can be improved much not only by using a sophisticated preconditioner. The smart choice of the initial approximations turns out to be equally important. In the nonstationary simulation, using the flow state from the previous time step seems to be a good idea. Surprisingly enough, this approach is rather disappointing. In this section we give a brief account of much better method proposed by Paul Fisher

In the general setting, consider the sequence of the large linear systems. These systems have the same SPD matrix $\mathbf{A}$, but different right-hand side vectors. The Fisher's projection method [11] can be described as follows:

Initiation:

$$\mathbf{A}\mathbf{x}^{(1)} = \mathbf{b}^{(1)} \rightarrow \mathbf{e}_1 = \mathbf{x}^{(1)} / \left\|\mathbf{x}^{(1)}\right\|_A, \quad \left\|\mathbf{x}^{(1)}\right\|_{\mathbf{A}} = \sqrt{\langle \mathbf{x}, \mathbf{x}\rangle_{\mathbf{A}}} \equiv \sqrt{\langle \mathbf{x}, \mathbf{A}\mathbf{x}\rangle}$$

for $k = 2, 3, \ldots$:

(a) Having the A-orthonormalized system of $k-1$ vectors $\mathbf{e}_1, \mathbf{e}_2, \ldots, \mathbf{e}_{k-1}$, we define the vector

$$\tilde{\mathbf{x}} = \sum_{j=1}^{k-1} \alpha_j \mathbf{e}_j$$

such that

$$\left\langle \mathbf{e}_j, \mathbf{b}^{(k)} - \mathbf{A}\tilde{\mathbf{x}} \right\rangle_{\mathbf{A}} = 0.$$

It is easy to show that

$$\alpha_j = \left\langle e_j, b^{(k)} \right\rangle.$$

(b) We seek the solution of the k-th system as $\mathbf{x}^{(k)} = \tilde{\mathbf{x}} + \mathbf{x}'$, where $\mathbf{A}\mathbf{x}' = \mathbf{b}^{(k)} - \mathbf{A}\tilde{\mathbf{x}} \equiv \mathbf{b}'$ is solved iteratively by the PCGM with the stopping criterion $\|\mathbf{r}'\|_2 / \left\|\mathbf{b}^{(k)}\right\|_2 < \varepsilon$. One can easily show that $\mathbf{r}' \equiv \mathbf{r}$.

(c) To continue the procedure, the next basic vector $\mathbf{e}_k$ has to be determined. To this end, we calculate the part of the solution orthogonal to the subspace spanned by the basic vectors generated so far

$$\mathbf{x}'_\perp = \mathbf{x}' - \sum_{j=1}^{k-1} \beta_j \mathbf{e}_j$$

where $\beta_j = \langle \mathbf{e}_j, \mathbf{x}' \rangle_A = -\langle \mathbf{e}_j, \mathbf{r}' \rangle$.

The following equivalent form, which avoids multiplication by the matrix $\mathbf{A}$, can be derived

$$\left\|\mathbf{x}'_\perp\right\|_A \equiv \sqrt{\langle \mathbf{x}', \mathbf{A}\mathbf{x}' \rangle} = \sqrt{\langle \mathbf{x}^{(k)}, \mathbf{b} - \mathbf{r}' \rangle - \sum_{j=1}^{k-1} (\alpha_j + \beta_j)^2},$$

and finally we get $\mathbf{e}_k = \mathbf{x}'_\perp / \left\|\mathbf{x}'_\perp\right\|_A$. If k becomes to large (say $k = K_{\max}$) the procedure is re-started: $\mathbf{e}_1 = \mathbf{x}^{K_{\max}} / \left\|\mathbf{x}^{K_{\max}}\right\|_A$.

Figure 8 shows the computational time per single simulation step, when the Fisher's method is implemented. In the presented case, the sequence is re-started every 100 time steps. After the restart, the computational time is quite large but it drops drastically after several steps. The average computational time per one integrations step is about 17 s (Pentium IV, 2.6 GHz, 1536 elements, $N_V = 6$, $N_P = 4$).

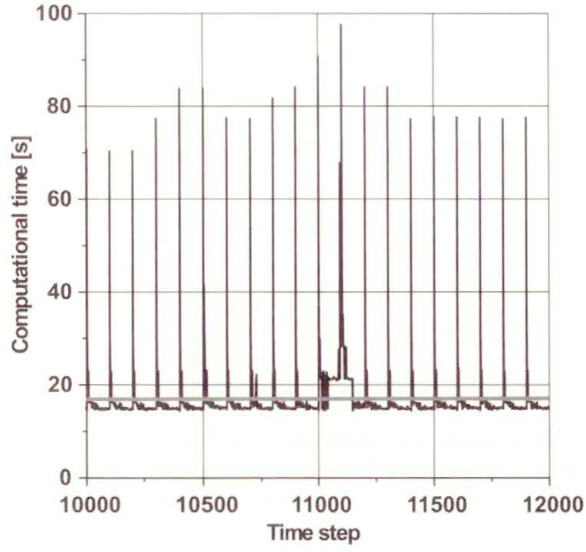

FIGURE 8. Performance of the Fisher's projection method—more details in the text

2.8. Sample Results, Encountered Difficulties and Further Development

2.8.1. Simulation of an unsteady flow in the T-shaped junction

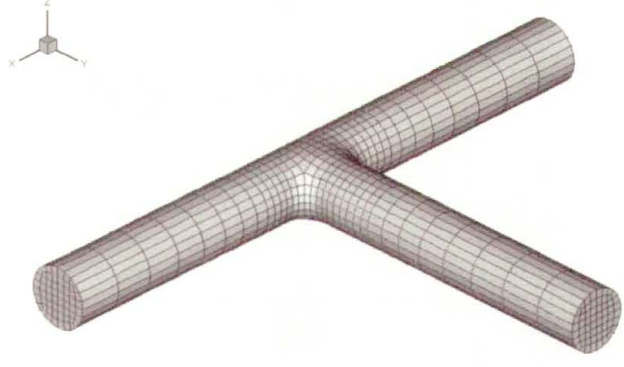

FIGURE 9. Hexahedral meshes for the T-shape pipe junction containing 1536 or 3048 spectral elements. The computations have been performed with (N_V, N_P)=(5,3) or (N_V, N_P)=(6,4).

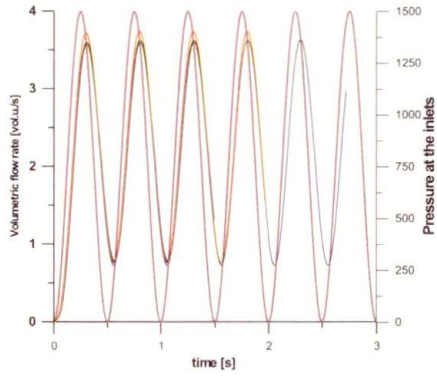

FIGURE 10. The volume flux of the test flow plotted as a function of time, calculated for different grids and collocation meshes: grid A with (5,3) mesh (blue line), grid A with (6,4) mesh (green line) and grid B with (5,3) mesh (red line). The black line corresponds to reference result obtained with FIDAP. The brown line depicts the time dependence of the prescribed inlet pressure.

2.8.2. Laminar flow in the T-junction accelerated from rest to a steady state

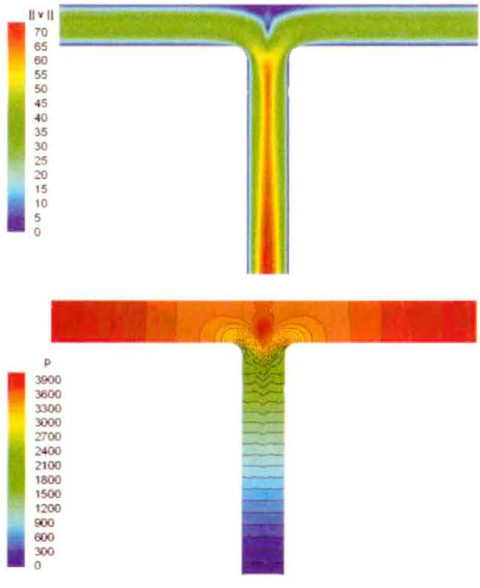

FIGURE 11. Contour maps of the steady-state velocity magnitude and the static pressure computed at the symmetry plane. The velocity units are cm/s; the pressure/density is shown in the bottom color map (the values are in cm^2/s^2).

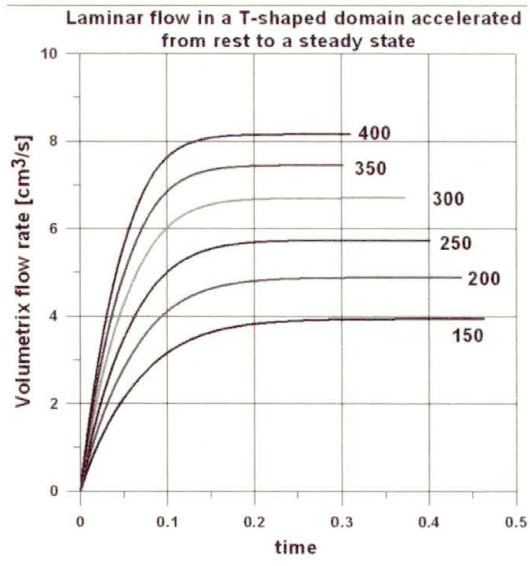

FIGURE 12. The volumetric flow rate as a function of time, for different driving pressure difference between the inlets and the outlet (the pressure units are Pa, the density is $10^3\,\mathrm{kg/m^3}$).

2.8.3. Laminar pulsatile flow in the simple model of the Blalock-Taussig shunt

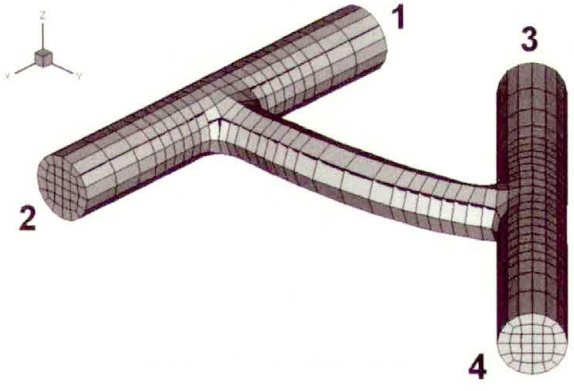

FIGURE 13. Geometric model of the BT shunt. In the figure, the smaller test grid of 1672 spectral elements is shown. The presented results have been computed for similar geometry but using the grid of 3760 spectral elements. The density of the internal collocation mess has been set to $(N_V, N_P) = (6, 4)$.

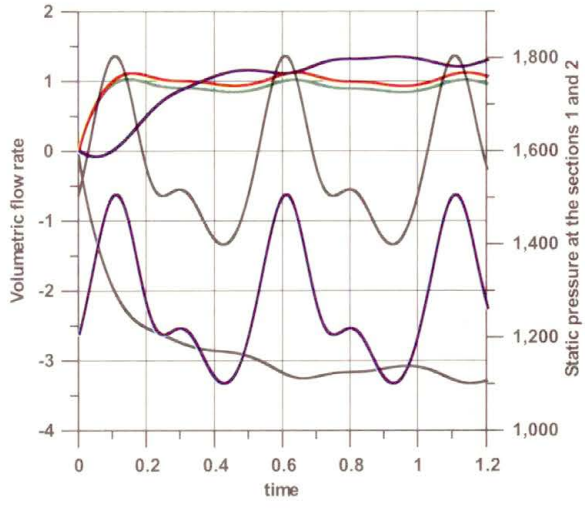

FIGURE 14. Temporal variation of the volume fluxes calculated for the BT shunt using AP-type conditions at all inlet/outlet sections. The black lines show the volume flux and static pressure at the inlet section 3. The blue lines represent the same data for the outlet section 4. The green and red lines show the temporal variations of the volume fluxes at the outlet sections 1 and 2, respectively. The pressure applied at these outlets was fixed in time and equal to zero.

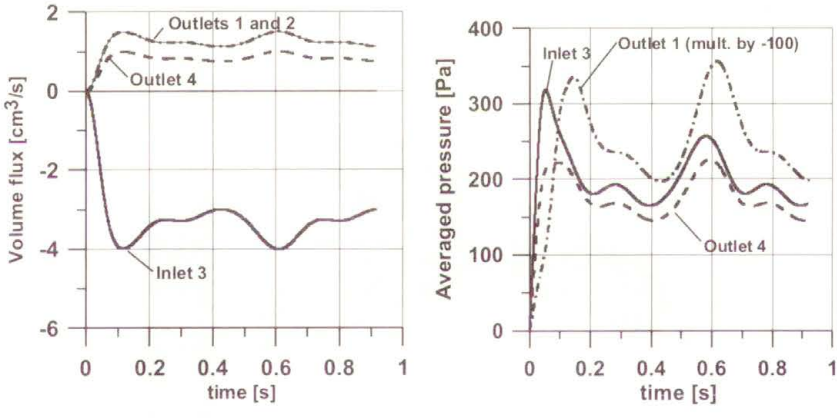

FIGURE 15. Pulsatile laminar flow in the BT shunt using VF-type inlet/outlet conditions. The left picture shows assumed volumetric flow rates at all I/O sections. The volume-flux distribution ratios are fixed in time and equal 37,5%, 37.5% and 25% for the outlets 1, 2 and 4, respectively. The right picture shows the computed temporal histories of the section-averaged static pressure at the I/O sections. Note the initial peak of the inlet pressure, which prevents the flow reversal at the outlet 4.

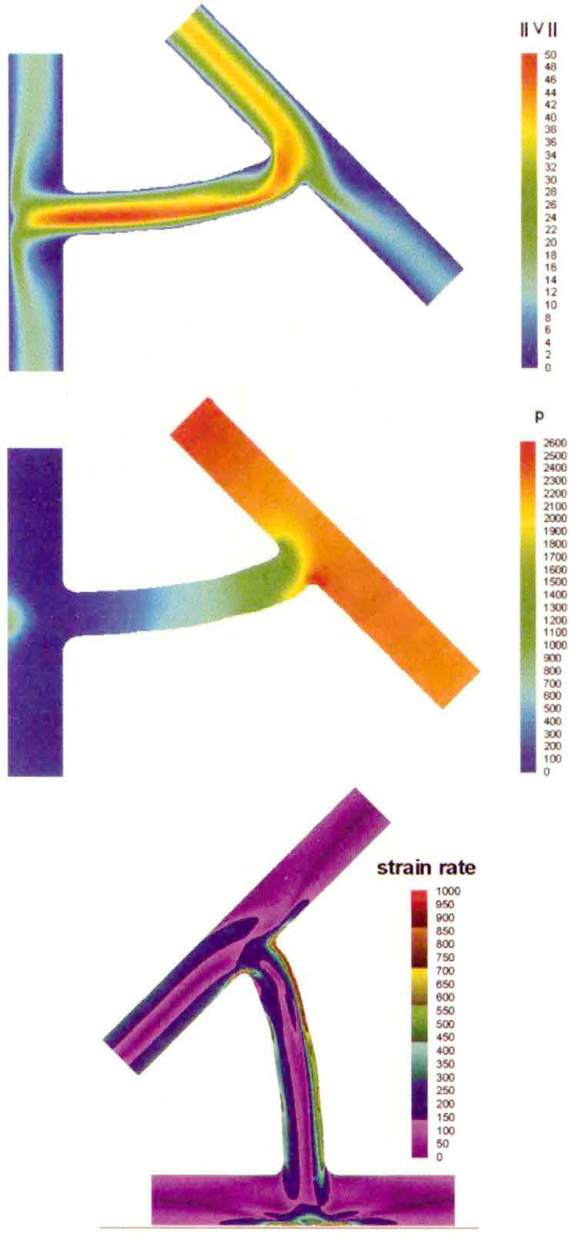

FIGURE 16. Top and center pictures: the contour plots of the velocity magnitude and the field of the static pressure to density ratio in the symmetry plane, computed for the time of the maximal flow rate. Bottom picture: the contour plot of the corresponding strain rate.

2.8.4. Encountered difficulties. Numerical instability of yet not understood origin appears at the inlet section. The scenario of the instability development can be characterized as follows.

First, rapid increase of a cross-flow (tangent) velocity is observed, which gives rise intensive generation of the "spikes" of the streamwise velocity. Eventually, the flow field quickly "blows up". The characteristic structure in the inlet velocity field is shown in Fig. 17.

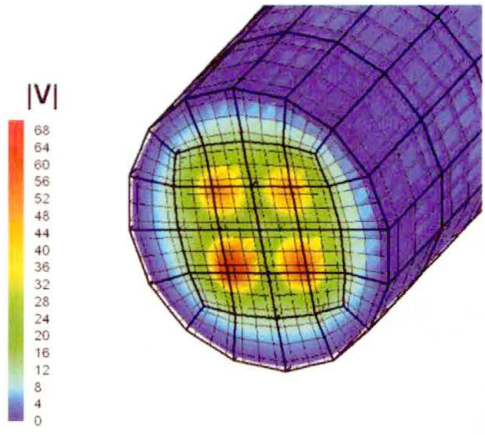

FIGURE 17.

2.8.5. Further development. The work of the improved versions of the spectral solver is in progress. In particular:

1. Experimental 2D codes with different inlet/outlet conditions (including zero tangent velocity, anyway!) are being developed (some undergraduate student's projects are carried out in the Faculty of Aeronautical and Power Engineering, Warsaw University of Technology). The main purpose is to investigate numerically stability properties of the spectral solvers with "deficient" inlet/outlet conditions.

2. Work on efficient parallelization of the solver(s) (with collaboration of the Interdisciplinary Center of Mathematical Modeling, University of Warsaw) will be continued.

3. Development of the spectral-element 3D nonstationary convection-diffusion solver based on preconditioned BiCGStab [8] iterations is in progress.

4. Implementation and computational tests of new high-order Yosida methods [18, 23] are planned.

3. Numerical Modeling of Blalock-Taussig Shunt Using Commercial CFD Package FLUENT

The last part of the lecture covered the clinical application of findings and assumptions given by the computational flow analysis in the group of patients undergoing the systemic to pulmonary shunting operation.

3.1. Clinical Background and General Considerations

Systemic to pulmonary shunt operation was first performed on November 20^{th} 1944 by Alfred Blalock. The patient undergoing that procedure was young girl suffering from congenital heart malformation of the type of tetralogy of Fallot (ToF). The most typical clinical finding in that subjects is cyanosis resulting form low oxygen saturation of arterial blood. Natural response to that condition is overproduction of the red blood cells (RBC) and augmentation of the hematocrit (HCT-RBC to plasma ratio) which leads to the strokes and haemorrhagic complications. The aim of the operation was to augment the oxygen saturation of the arterial blood by redirecting part of the blood flowing through the systemic circulation back to the pulmonary circulation. The concept was developed by Hellen Brook Taussig, cardiologist, who noticed deterioration of clinical status in the subjects suffering form ToF at the time of natural occlusion of the ductus arteriosus.

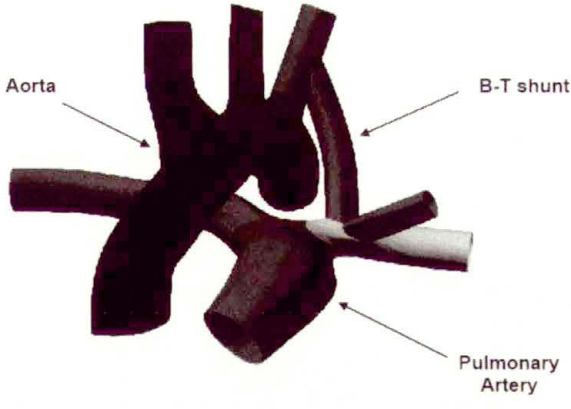

FIGURE 18. The general overview of the localization of B-T shunt

Contemporarily the modified Blalock-Taussig anastomosis is very important first stage of palliation in many forms of congenital heart malformations, especially requiring Fontan-like circulation as a final solution. The patency of first stage palliation (mBT) delimits the time step length and the time interval for the further surgical interventions.

3.2. Definition of the Model Geometry

Due to the complication of the geometry of the aortic arch and the pulmonary artery branching the volume of the model submitted for further investigation was greatly reduced and simplified.

(a) (b) (c)

FIGURE 19. (a) Complete volume of the great vessels and prosthetic shunt, (b) abstracted region of the systemic to pulmonary shunt, (c) geometry of the numerical model

Final geometry was meshed with standard domain meshing commercial software Gambit™, [25]. The obtained tetrahedral mesh consisted of 90 829 cells, 187 793 faces and 18 367 nodes. Total volume of the model was: $1.85929 \times 10^{-6}\,\mathrm{m}^3$ (1,86 ml).

3.3. Definition of Boundary Conditions

Boundary conditions were also greatly simplified. The walls of the model were defined as rigid with no slip condition applied. Fluid flowing through the domain was defined as Newtonian viscous with the following parameters: $\rho = 1060\,\mathrm{kg/m}^3$ and $\nu = 0.004\,\mathrm{kg/ms}$.

SA inflow (red arrow in Fig. 20) is defined as time dependant mass flow inlet. The user defined function is equipped with basic driving curve of mass flux changes and the linear interpolation between the given time instants is used. The flow direction is set to be normal with respect to the inlet surface and the distribution of the mass flux (ρv_n) is assumed uniform.

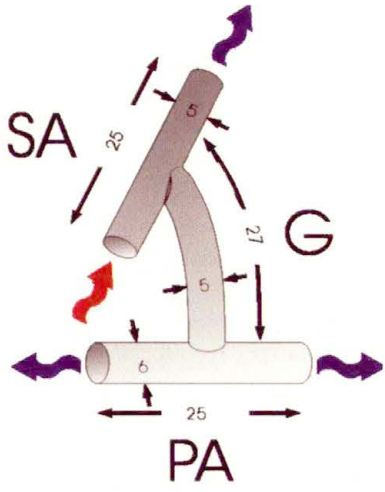

FIGURE 20. Dimensions in mm and flow directions in the B-T shunt computational model

- SA outlet (blue arrow in Fig. 20) was defined as: outflow with flow rate weighting = 0.5,
- PA outlets (blue arrows) were defined as: outflow with flow rate weighting = 1.

Such definition results in flowing flow distribution:

- 20% of volumetric flow continues towards the SA outlet,

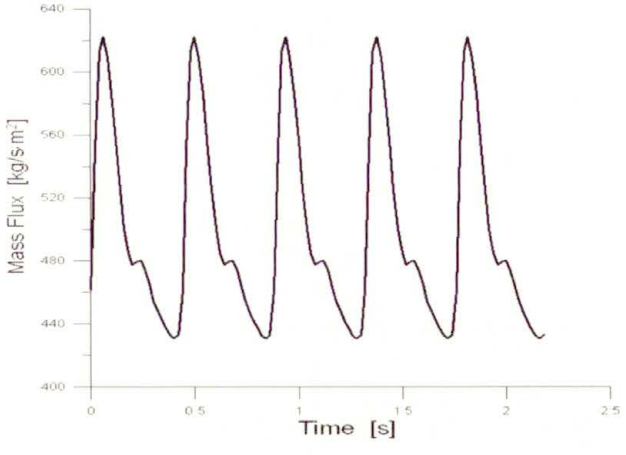

FIGURE 21. Mass flux driving curve at the SA inlet

- 80% of the volumetric flow is redirected towards both PA outlets,
- PA outlets flow was equally split between both of them.

The outflow distribution was chosen according to the clinical findings based upon postoperative echocardiography.

With the outflow conditions, all flow parameters (except pressure) were extrapolated to the outflow section from within the domain in such a manner that the diffusion fluxes are zero (homogeneous Neumann b.c.). Such approach is justified providing that the outflow is reasonably close to a fully-developed state.

3.4. Solver Settings

The most of the default values were applied for solving the flow equations inside the defined geometry.

- Viscous model: laminar,
- Pressure-velocity coupling: simple,
- Fixed time step: $\Delta t = 2 \times 10^{-4}$ s,
- Convergence criterion: $\varepsilon = 10^{-7}$.

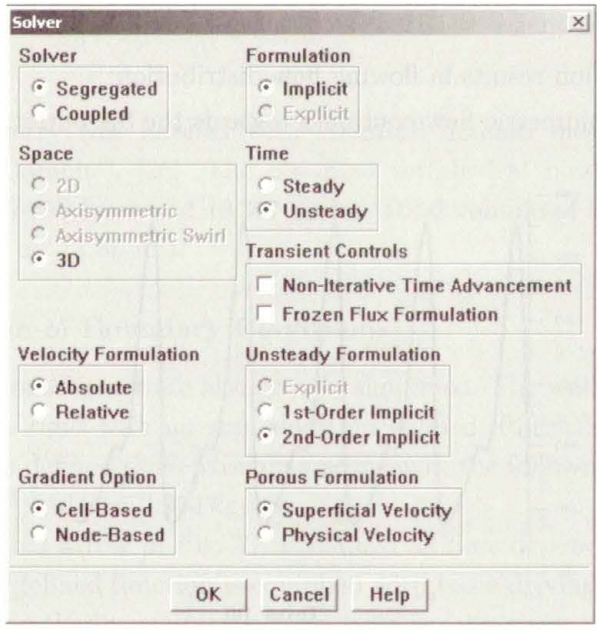

FIGURE 22. Solver settings—FLUENT 6.2.18

3.5. Results and Conclusions

Computer models included left subclavian artery, graft, and left pulmonary artery, and represented the average geometry of the graft in two groups of patients. The size of the blood vessels was the same in both models, but the graft was longer and narrower in model B (clotted grafts) than in model A (patent grafts). Shear stress fields were calculated, and the volume within the model with high shear rate (over 2500 1/s) was determined, in different phases of the cardiac cycle.

About 80% of inflowing blood was directed to the pulmonary circulation. In both models we observed a large recirculation region at the inlet to the graft accompanied by a high shear stress region at the opposite wall of the graft. The region of high stress was less than 0.5% of total volume of the system in model A (patent grafts), and over 4% of total volume in model B (clotted grafts).

Narrow and long grafts create flow patterns with high shear stress that promote platelet activation leading to augmented risk of clot formation. Therefore the graft geometry may be one of crucial factors in mBT anastomosis failure.

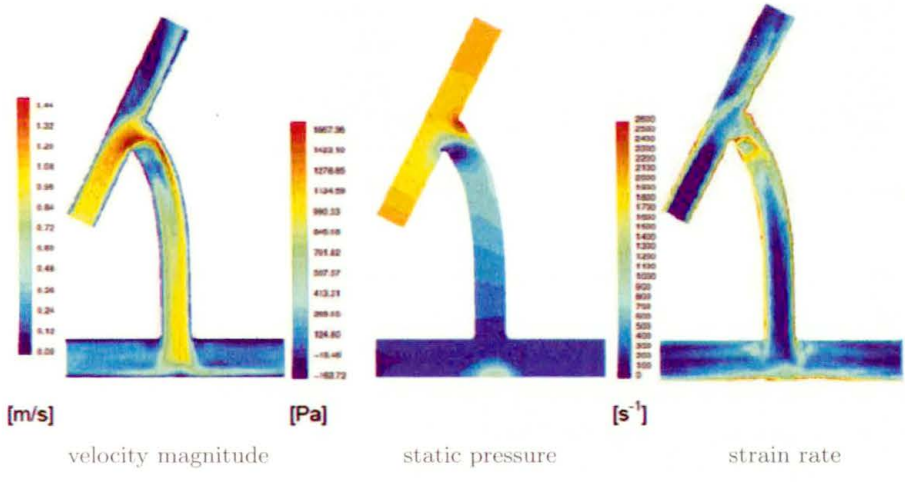

FIGURE 23. Results obtained during systolic phase of the simulation

The most important findings from the medical point of view were the results being in best agreement with the findings common in invasive and non invasive clinical examinations.

The best example of that was perfect explanation of the pressure loss at the inlet of the graft commonly found in hemodynamic postoperative study of the patients undergoing the mBT shunting.

The second important finding was the visualization of the high shear stress regions at the inlet of the prosthetic vessel. Shear stress is considered the most important mechanical factor directly influencing biochemical reactions like thrombosis and intimal hyperplasia in vascular system.

Numeric models gave the unique opportunity to study in "patient safe" environment such conditions like:

- Hydraulic pressure loss in the B-T shunt,
- regions of high shear rate can be localized,
- vulnerability of the flow to the geometry of the proximal anastomosis.

During the evaluation period of the results we found some quasi-compressibility occurring in solving method although the setting of the solver explicitly was set to non-compressible.

TABLE 4. "Quasi-compressibility" effect of the solver results in relatively large error in instantaneous volumetric flux balance

Inlet/outlet	Mass flow rate [g/s]	Vol. flow rate [cm^3/s]	Avg. density [g/cm^3]
1 (Out)	4.69714	4.297437	1.09301
2 (Out)	4.69714	4.291925	1.09441
3 (In)	−11.74285	−10.04857	1.16861
4 (Out)	2.34857	2.142215	1.09633
Σ	0.0	−0.683007	—

From the computational point of view some safeguards and pitfalls had to be mentioned for the "non engineer" user of the commercial packages. All of the results obtained from the CFD methods has to be carefully evaluated and the sole judge of their applicability for the medical doctor has to be common sense and critical analysis.

Acknowledgement

This project was funded by Polish Committee of Scientific Research, grant 7 T11F 018 20.

References

1. R. ARIS, *Vectors, Tensors and the Basic Equations of Fluid Mechanics*, Dover, New York 1962.
2. G.K. BATCHELOR, *An Introduction to Fluid Dynamics*, Cambridge University Press, Cambridge 1967.
3. J.P. BOYD, *Chebyshev and Fourier Spectral Methods*, 2nd Ed., Dover, Mineola, New York 2001.
4. C. CANUTO, M.Y. HUSSAINI, A. QUARTERONI, and T.A. ZANG, *Spectral Methods in Fluid Dynamics*, Springer Verlag, Berlin/New York 1988.
5. M. GUNZBURGER, *Finite Element Methods for Viscous Incompressible Flows: A Practical guide to Theory, Practice and Algorithms*, Academic Press, Boston, 1989.
6. G. KARNIADAKIS and S.J. SHERWIN, *Spectral/hp Element Methods for CFD*, Oxford University Press, 1999.
7. M.O. DEVILLE, P.F. FISHER, and E.H. MUND, *High-Order Methods for Incompressible Fluid Flow*, Cambridge University Press, 2002.
8. Y. SAAD, *Iterative Methods for Sparse Linear Systems*, 2^{nd} Ed., SIAM, 2003.
9. J. CAHOUET and J.P. CHABARD, *Some Fast 3D Finite Element Solvers for the Generalized Stokes Problems*, Int. J. Numer. Meth. Fluids, **8**:869–895, 1986.
10. W. COUZY and M.O. DEVILLE, *Spectral-Element preconditioners for the Uzawa pressure operator applied to incompressible flows*, J. Scientific Computing, **9**(2):107–122, 1994.
11. P.F. FISHER, *Projection techniques for iterative solution of* $\mathbf{Ax} = \mathbf{b}$ *with successive right-hand sides*, Comput. Methods. Appl. Mech. Eng., **163**:193–204, 1998.
12. J.G. HEYWOOD, R. RANACHER, and S. TUREK, *Artificial boundaries and flux and pressure conditions for the incompressible Navier-Stokes equations*, Int. J. Numerical Methods in Fluids, **22**:325–352, 1996.
13. G. KARNIADAKIS, M. ISRAELI, S.A. ORSZAG, *High-Order Splitting methods for the Incompressible Navier-Stokes Equations*, J. Comp. Phys., **97**:414–443, 1991.
14. Y. MADAY, A.T. PATERA, and E.M. RONQUIST, *An operator-integration-factor splitting method for time-dependent problems: Application to incompressible fluid flow*, J. Sci. Comput., **5**:263–292, 1990.
15. Y. MADAY, D. MEIRON, A. PATERA, and E.M. RONQUIST, *Analysis of iterative methods for the steady and unsteady Stokes problem: application to spectral element discretizations*, SIAM J. Sci. Comput. **14**(2):310–337, 1993.
16. E.M. RONQUIST, *A domain decomposition method for elliptic boundary value problems: Application to unsteady incompressible fluid flow*, in the Proceedings of 5^{th} Conference on Domain Decomposition Methods for Partial Differential Equations, D.E. Keyes et al. [eds.], pp.545–557, 1991.

17. J. SZUMBARSKI, P. OLSZEWSKI, A. STYCZEK, J. ROKICKI, Z. MAŁOTA, and K. WAWRUCH, *Computations of an Unsteady Viscous Flow in a Three Dimensional System of Ducts*, J. Theoretical Appl. Mech., **42**(1)—Part 1, and (4)—Part 2, 2004.

18. A. QUARTERONI, F. SALERI, and A. VENEZIANI, *Analysis of the Yosida method for the incompressible Navier-Stokes equations*, J. de Mathematiques Pures et Appliques, **78**: 473–503, 1999.

19. W. COUZY, *Spectral Element Discretization of the Unsteady Navier-Stokes Equations and Its Iterative Solution on Parallel Computers*, Ph.D. Thesis, Ecole Polytechnique Federale De Lausanne, No 1380, 1995.

20. *Lecture notes of the Summer School on the Modelling of the Cardiovascular System*, (org. A. Quarteroni), EPFL, Lausanne, 25–30 August 2003.

21. A. QUARTERONI and L. FORMAGGIA, *Mathematical Modelling and Numerical Simulation of the Cardiovascular System*, MOX Rep. 1, 2002.

22. A. VENEZIANI and C. VERGARA, *Flow Rate Defective Boundary Conditions in Haemodynamics Simulations*, MOX Rep. 35, 2003.

23. P. GERVASIO, F. SALERI, and A. VENEZIANI, *Algebraic Fractional Step Schemes with spectral methods for the Incompressible Navier-Stokes Equations*, MOX. Rep. 61, 2005.

24. L. FORMAGGIA, J.F. GERBEAU, F. NOBILE, and A. QUARTERONI, *Numerical treatment of defective boundary conditions for the Navier-Stokes equations*, EPFL, Departement de Mathematiques, Preprint 20, 2000.

25. *Fluent 6.2 User's Guide*, Fluent Inc., 2005.